Heat-Transfer Gauge Arrays for Identifying Spot Initiation in Hypersonic Transitional Boundary Layers

David J. Mee *
The University of Queensland, Brisbane, Queensland, 4072, Australia

Sreekanth Raghunath†
National University of Singapore, Singapore 119260, Republic of Singapore

Matthew McGilvray‡
University of Oxford, Oxford, England OX2 0ES, United Kingdom

The initiation and growth of turbulent spots in transitional hypersonic boundary layers can influence the transition length and the distribution of heat transfer and skin friction through the transitional region. There is debate in the literature about whether spots initiate in a small band at the start of transition or throughout the transitional region. This paper presents a new design of arrays of thin-film heat transfer specifically designed to detect whether spots initiate in a small band. The gauges were arranged in two spanwise rows at different streamwise locations and were tested on a 7° blunt cone in the T4 Stalker Tube. It is shown that such instrumentation is capable of identifying that some spots initiate between the rows when other spots have already formed upstream of the first row. This demonstrates that the breakdown of laminar boundary layers is not concentrated in a region of small streamwise extent in the current hypersonic flows.

Nomenclature

f = frequency

h = enthalpy

l = surface distance from stagnation point on blunt tip

$\dot{q}$ = heat transfer rate

R = resistance of gauge

Re = Reynolds number

St = Stanton number (eq. 1)

T = temperature

u = flow speed

*Emeritus Professor, Centre for Hypersonics, School of Mechanical and Mining Engineering, Associate Fellow AIAA.
†Currently Honorary Fellow, Centre for Hypersonics, School of Mechanical and Mining Engineering, The University of Queensland.
‡Associate Professor, Oxford Thermofluids Institute, Department of Engineering Science, Osney Mead, Southwell Building. Member AIAA

V = voltage across thin film

x = axial distance from the from virtual apex of sharp cone

α_R = temperature coefficient of resistance

γ = intermittency

λ^* = transition length scale (Eq. 4)

μ = dynamic viscosity

ρ = density

Subscripts

0 = value before flow arrival

l = based on l

m = mean value

s = nozzle-supply

t = value at the start of transition

w = value at the wall of the cone

∞ = freestream condition

Superscripts

$'$ = r.m.s. value

I. Introduction

It has been observed that the process of boundary layer transition in hypersonic flows can include the initiation and growth of turbulent spots (e.g. [1][2][3]). If the rates at which spots grow in both the streamwise and lateral directions are known, then the length of the transitional region can be determined if the locations and the rate of spot initiation are known (e.g. [4] [5] [6]). Therefore it is useful to know where spots are initiated and the rate at which they are generated.

Much of the research on the initiation of turbulent spots has been done in incompressible flows and in flows around turbomachinery blading. Emmons [7] original work on modeling the transition process assumes that turbulent spots form randomly with equal probability throughout the transitional region. This is referred to as "distributed breakdown" by Johnson and Dris [8].

Narasimha [9] developed a 'generalized intermittency distribution' that is based on the hypothesis of 'local' or 'concentrated' breakdown. This hypothesis is that 'spots form at a preferred streamwise location randomly in time and

in cross-stream position'. Under this hypothesis, turbulent spots are all initiated at the start of the transitional region. This is shown schematically in Fig. 1a. Intermittency distributions obtained using this model have been found to provide good fits with experimental results in low-speed [9] and hypersonic [2] flows.

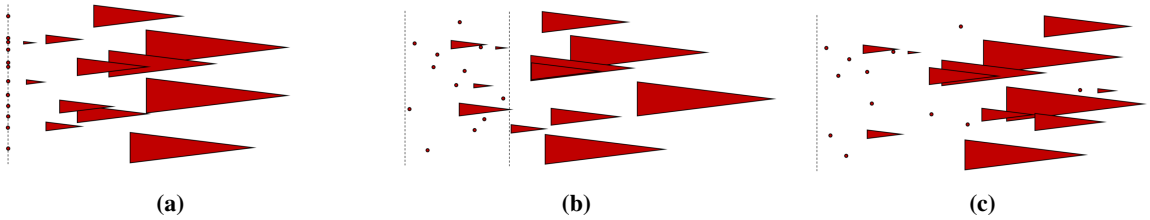

Fig. 1 Schematic diagram showing different types of breakdown. The vertical dashed line shows the most upstream location where spots initiate. Locations of initiation of spots is shown by red circles; spots are shown as red triangles. (a) Concentrated breakdown. (b) Quasi-concentrated breakdown. (The second vertical line shows the most downstream location where spots initiate.) (c) Distributed breakdown (with higher probability of spot initiation near the start of transition).

An alternative model is that spots may be initiated over a limited part of the transitional region. This is referred to as "quasi-concentrated breakdown" by Zhang et al.[10] and is shown schematically in Fig. 1b. In fact, Narasimha[9] suggests that the idea of concentrated breakdown cannot be literally correct but that spots are initiated in a "belt" across the flow, the streamwise length of which is small compared with the streamwise extent of the transition zone. The restriction that the region is small in streamwise extent is not required in the quasi-concentrated breakdown model. Another alternative is that spots form in regions of the transitional zone with a probability dependent on the position within the zone. An example of this is shown in Fig. 1c where there is a higher probability of spot formation towards the start of transition. In this example, where there is a low probability of spots initiating late in the transition zone, the influence of these smaller spots on intermittency may not be large.

As noted by Narasimha[9], a good way to differentiate between whether a flow has concentrated or distributed breakdown is that small, newly-generated spots will be evident well into the transitional region for the latter case, as shown in Fig. 1c.

There is also evidence that, when the breakdown in not concentrated, turbulent spots are less likely to form in the calmed region behind turbulent spots[11]. This would lead to more spots being initiated earlier in the transitional region than later because there would be more and larger calmed regions behind spots later in the transitional region.

The goal of the present investigation is to identify whether concentrated breakdown occurs in transitional boundary layers formed on conical models in hypersonic shock-tunnel flows. In order to achieve this, an experiment was devised to detect turbulent spots using two spanwise arrays of thin-film heat-transfer gauges, with each array at a different distance from the apex of the cone. If turbulent spots are present at the upstream array, they should be detected at the downstream array also. If any spots are detected at the upstream array and new spots are detected at only the downstream array, then these spots must have formed between the two arrays and the breakdown can't be truly concentrated. The design of the

arrays also leads to useful visualisation of the passage of spots across the rows of gauges.

The design and manufacture of the arrays of thin-film gauges are described. The facility used to test the gauges, the T4 Stalker Tube at The University of Queensland, and the conical model are then detailed. Results are then presented and discussed and conclusions are drawn.

II. Arrays of Thin-Film Heat-Transfer Gauges

Thin-film heat-transfer gauges (TFHTG) have been used for measurement of heat transfer to the surfaces of models in various types of facilities for many years; see reviews by Schultz and Jones[12] and Alam and Kumar[13]. They are particularly suitable for hypersonic impulse facilities that have a very short flow establishment time and a short flow duration and can be designed to have response times of the order of microseconds.

Streamwise lines of thin-film gauges have been used to identify turbulent spots and their growth rates in high-speed flows (e.g. [14][2]). However, it is not possible to determine where spots initiate from such lines; unless all spots are generated along the line of gauges, only the edges of spots may be detected as they sweep over the sensors. Spanwise rows of gauges have also been used (e.g. [15][3]) and they can give a good indication of the sizes and shapes of spots. However, there are gaps between gauges where spots of small spanwise extent may pass undetected. Some researchers have used arrays of thin-film or co-axial thermocouple gauges covering the surface in both streamwise and spanwise directions (e.g. [16][5]). Again, some spots may not be detected if they pass between the locations of sensors. Full coverage of the heat transfer on a surface can be obtained using temperature-sensitive paints (TSPs) and these have been applied to study transition in hypersonic flows (e.g. [17][18]). The response time of such TSP systems is not sufficient to detect individual, naturally occurring turbulent spots but averages of periodically-generated artificial spots have recently been studied using TSPs [19]. The gauges used here were designed to provide the temporal resolution needed to detect turbulent spots with a spatial resolution designed to detect all spots passing over a spanwise line.

The types of arrays of gauges used in the present study and their design and manufacture have been under development in Oxford University's Thermofluids Institute for the past few decades[20][21]. The TFHTGs used here were platinum films connected between copper leads on a 50-μm thick kapton (polyimide) substrate. The kapton substrate, including the gauges and leads, used in the present tests (450×280 mm) is the largest that has been manufactured by the Oxford group.

The pattern of copper leads was formed by photo etching them from a film of kapton that was laminated with a 30-μm thick layer of copper. Most of the copper leads were 1.5 mm wide but, in some places, only 1.0 mm wide. The platinum thin films, estimated to be 30 nm thick, were deposited between the copper leads.

A 7° semi-angle cone was chosen as the test model. The goal of the design of the arrays of TFHTGs used here was to have two uninterrupted rows of gauges that spanned about one-third of the circumference of the cone at two distances from the apex of the cone. The extent of the downstream array should be sufficient to cover the same conical rays from

the apex of the cone as the upstream array. Another goal was that the two rows of gauges should be located within the transitional region of the boundary layer formed on the cone. The aim of having uninterrupted rows of gauges is so that any turbulent spots that pass over an array, within the span of the gauges, will be detected. If any turbulent spots are detected on the first array of gauges, they should propagate and grow before reaching the second array of gauges and be detected there also. If these spots were all initiated within a band of small streamwise extent, as in the concentrated breakdown hypothesis, then there should be no spots detected at the second row of gauges that can't be traced back to those detected at the first row.

The design of the TFHTG arrays is shown in 2. Each of the 66 platinum thin-film gauges has a sensing area 0.6 mm wide and 4 mm long. There are two circumferential rows of gauges and one streamwise row of gauges. The sheet of instrumentation was designed so that it could be attached to and would wrap around the entire circumference of a 591-mm long 7° semi-angle cone starting 360 mm from the apex and extending to the end of the cone.

The circumferential rows of gauges are actually made up of two lines of gauges. The spacing between the centre of each line is 1 mm. This can be seen more clearly in the photograph zoomed in around the middle of the second row of gauges in Fig. 3. Parts of the platinum were deposited over the copper to make a good connection and the 4×0.6 mm sensing region is highlighted for one of the gauges in the figure. Note that the gauges are arranged so that the end of the sensing region of a gauge in one line aligns circumferentially with the start of another gauge in the next line. This continues so that there is a complete row where heat transfer is measured with a resolution of 4 mm, the length of the gauges. If a turbulent spot has a spanwise extent of less than the length of a gauge, it will still be detected but the heat-transfer rise will not be to the full extent that would be obtained if the spot covered the entire gauge.

The streamwise row of eight gauges, seen towards the top of the pattern in Fig. 2, was designed to give an indication of where transition was occurring on the test model. The results from those gauges are not discussed in the present paper. When attached to the conical model, the first row of circumferential gauges was comprised of a line of 12 gauges at x = 399.5 mm and 13 gauges at x = 400.5 mm. Here, x is the axial distance from the virtual apex of the cone if it was sharp. These are referred to as lines 1 and 2 and the complete set as row 1, or the "400 mm row". The surface distance from the stagnation point on the blunt nose to this middle of this row was l = 398 mm. The second row consisted of 16 gauges at x = 499.5 mm and 17 gauges at x = 500.5 mm from the apex. These are referred to as lines 3 and 4 and the complete set as row 2, or the "500 mm row". The surface distance to the middle of this row was l = 499 mm.

The value of $\sqrt{\rho c k}$ for kapton is taken from the experiments of Piccini et al. [22] to be 490 $\mathrm{Wm^{-2}K^{-1}s^{0.5}}$. Taking $\sqrt{\rho c k}$ for platinum to be 14000 $\mathrm{Wm^{-2}K^{-1}s^{0.5}}$, the analysis in Schultz and Jones[12], that they use to estimate the errors in surface heat transfer due to the presence of a thin metallic layer, can be used to find that the 10% to 90% rise time for a step change in heat transfer for a 30-nm platinum film is 1 μs.

The thin-film gauge power supplies and amplifiers used were designed in house. They pass a small constant current (of order 10 mA) through the platinum films during the test time and sense and amplify the voltage drop across the film

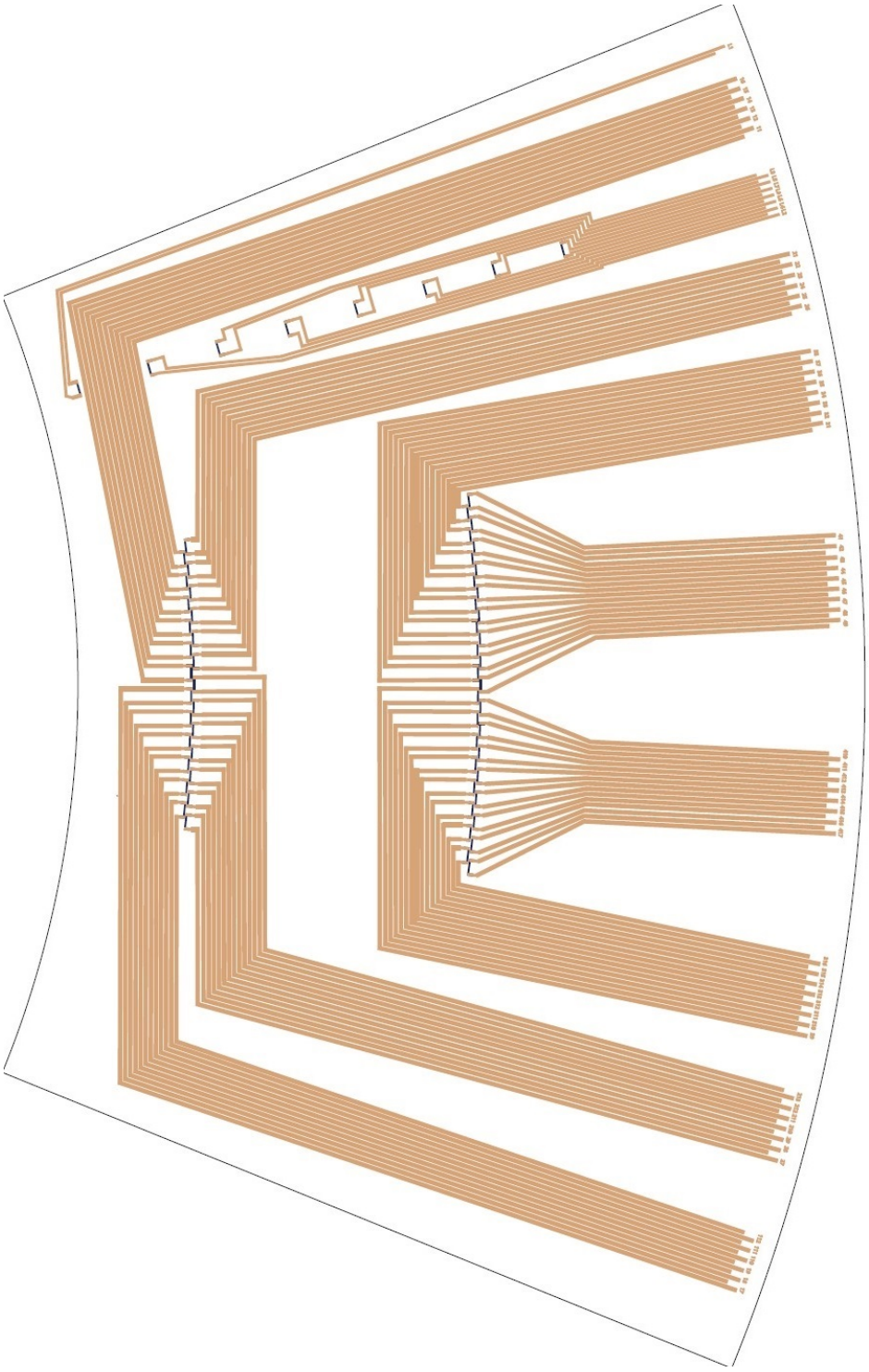

Fig. 2 Design of the arrays of TFHTGs for detecting where turbulent spots initiate on a 7° semi-angle cone. The platinum gauges are shown in black and the copper leads in brown. When attached to the cone, flow is from left to right.

which changes with the temperature of the film. The resistance change of the film with temperature was modelled as $\Delta R = \alpha_R R_0 \Delta T$. If the voltage before the flow arrives is V_0, the change in temperature during the test can then be found

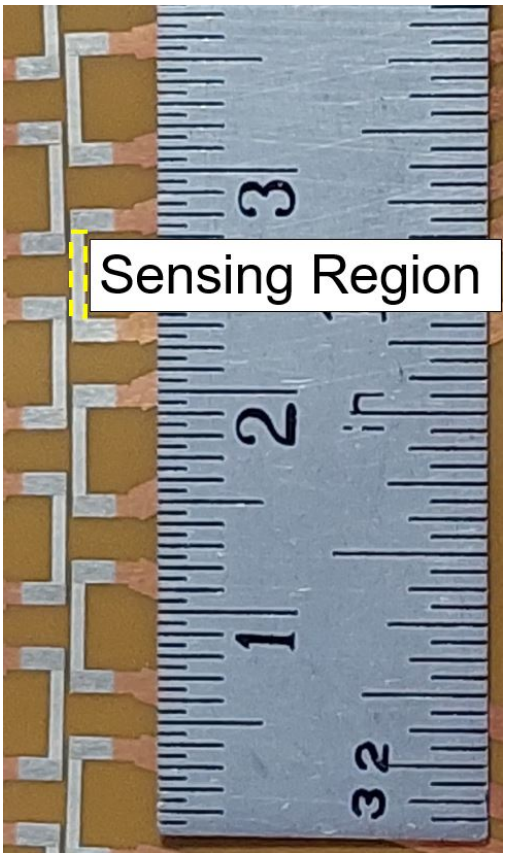

Fig. 3 Photograph showing detail around TFHTG array.

from the change in voltage, ΔV, from $\Delta T = \frac{1}{\alpha_R}\frac{\Delta V}{V_0}$. The heat transfer rates were inferred from the change in surface temperature assuming a semi-infinite substrate using the method of Oldfield[23].

The kapton film with the array of TFHTGs on it was attached to the model using 3M double-sided tape. This makes it relatively easy to install the instrumentation on the model although some care is needed to ensure that no air bubbles are trapped between the film and the surface. The total thickness of the film and glue layer was approximately 110 μm. In determining the heat transfer rate from the change in surface temperature of the platinum film, it is assumed that the thermal properties of the glue layer are similar to those of the kapton [21]. The thermal penetration depth is taken to be the depth to where the temperature and heat transfer rates are around 1% of the value at the surface[12]. With the 110-μm thick substrate, the time for thermal penetration to reach the bottom of the glue layer is around 7 ms. Therefore, the semi-infinite assumption for inferring the surface heat transfer rate is appropriate for times up to 7 ms after flow arrival in the experiments.

In general, the resistances of the gauges increased over the duration of the test campaign. This is attributed to erosion of the gauges during the test flow and as the driver gas passed over the model after the test flow. In a pilot study, gauges of the same construction were attached to a flat surface inclined at 15° to the oncoming flow. Nine shots were fired at

the same flow conditions. The resistances of gauges in those tests also increased as the campaign continued, but by more than those of the gauges in the cone tests. It is proposed that this is due to more erosion of the gauges on the surface at a higher inclination angle to the oncoming flow in the pilot study. Despite the changes in resistances of the gauges in the pilot study, the heat fluxes inferred from the gauges were repeatable across the nine shots by taking the increase in starting resistance, R_0, into account and assuming that α_R remained unchanged.

III. The Experiments

A. The T4 Stalker Tube

The experiments reported here were performed in the T4 Stalker Tube (a free-piston-driven, reflected shock tunnel)[24] at The University of Queensland. T4 can generate flow at total enthalpies from 1.5 to 12 MJ/kg and nozzle supply pressure from 5 to 80 MPa. Test times vary with flow conditions from one to several milliseconds.

In the present test campaign, the unit Reynolds number of the nozzle exit flow was varied from 2.1 to 13.6 million/m in order to vary the locations on the model where the flow was transitional. The Mach 7 nozzle[25][26] was used and the total enthalpy was varied between 2.2 and 3.3 MJ/kg. The nozzle-supply pressure was varied from 5 to 25 MPa. An example of a nozzle-supply pressure trace is shown in Fig. 4. The data acquisition system was triggered from the rise in pressure of this nozzle-supply pressure sensor, located just upstream of the end of the shock tube. Time zero is when the system triggered. At the conditions of the present tests, it took about 1.5 ms for the flow to establish in the nozzle and over the model. The nozzle-supply pressure was then approximately constant for another 2 ms before the pressure dropped away. This 2 ms period was taken as the test window.

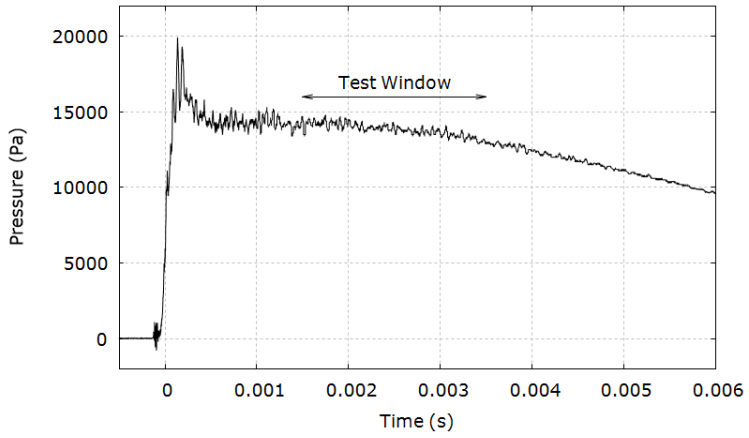

Fig. 4 Example nozzle-supply pressure trace (Shot 12181, Re_∞ = 5.1 × 10^6 m^{-1}; h_s = 2.8 MJ/kg).

The conditions of the flow in the nozzle-supply region and at exit of the nozzle were determined using the in-house code estcn, an update to the state-to-state shock tube solver, ESTCj [27]. This takes as input the initial filling conditions of the shock tube gas, the speed of the primary shock, the measured pressure in the nozzle-supply region and the

ratio of Pitot pressure at the exit of the nozzle to the nozzle-supply pressure. It then determines the nozzle-supply and nozzle-exit conditions assuming equilibrium gas chemistry. Equilibrium chemistry is suitable for the relatively low-enthalpy conditions of the present tests.

It is well established that freestream noise can influence boundary layer transition (e.g.[28]), so it is appropriate to document the freestream flow fluctuation levels for the tunnel used in the present experiments. The noise in the flow exiting the Mach 7 nozzle was measured in a separate study by Ramprakash [29] using Focused Laser Differential Interferometry (FLDI). The r.m.s. of the density fluctuations normalised by the mean density are shown in Fig. 5 for octave band centre frequencies from 31.5 kHz to 500 kHz. Results for a shot at a nozzle-supply enthalpy of 1.6 MJ/kg are shown. It can be seen that the density fluctuations decrease with increasing frequency and that the normalised level is at or below 0.5% in all octave bands.

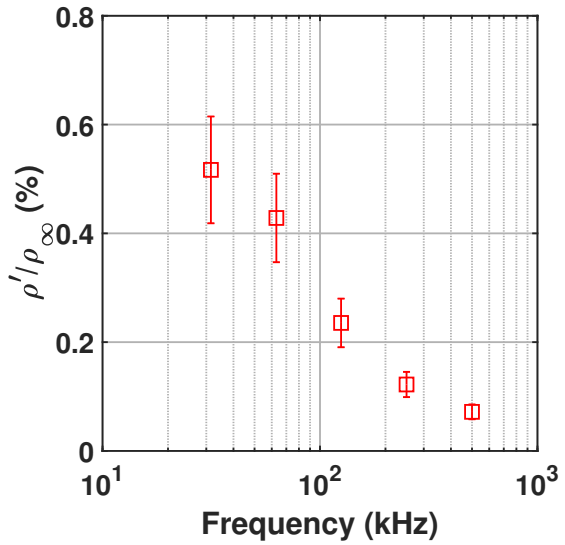

Fig. 5 FLDI measurements of the r.m.s. of the density fluctuations normalised by the mean density for T4's Mach 7 nozzle [29]. Re_∞ = 14.7 $\times 10^6$ m^{-1}; h_2 = 1.6 MJ/kg.

It is shown by Jewell et al. [30] that particulates in the T5 Stalker tube at Caltech, left over from previous experiments, can cause earlier transition if they impact the surface of the model during the test time. The effects of particulates on transition in supersonic flows is analysed by Federov [31]. In order to minimize the possible effects of such particulates in the present experiments, the T4 shock tube and nozzle were cleaned thoroughly before each test and nylon buffers were used instead of the usual rubber buffers in T4.

B. The Test Model

The test model was a blunted 7° semi-angle cone. The tip of the cone was spherically blunted to a radius of 1.55 mm. The axial length of the cone was 591 mm. The ratio of bluntness to cone length was chosen to be similar to (15% larger

than) that of the blunted 7° semi-angle cone flown at Mach 7 in the HIFIRE-1 boundary-layer transition experiment [32]. The first 80 mm from the apex of the cone was made from stainless steel and the rest of the cone was aluminium. A photograph of the model prior to installation of the gauges is shown in Fig. 6a. A 0.11-mm backward-facing step was machined into the surface at 360 mm from the apex. This was to accommodate the kapton film and its adhesive backing (a total of 0.11 mm thick) so that there was no step at the leading edge of the kapton film. Therefore, any influence of the installation of the gauges on the flow over the cone was minimised. A 20-mm conically tapered section at the end of the cone was included so that twisted-pair cables could be soldered to the ends of the copper leads for the gauges. A stainless-steel sting was attached at the base of the cone and this was held in the T4 sting mounting system from the ceiling of the test section. The wiring for the TFHTGs passed through slots in the sting, through the sting mounting system and out through feed-through ports to signal conditioners outside the tunnel. A photograph of the model with the gauges and wiring attached and installed in the test section of the T4 Stalker Tube is shown in Fig. 6b.

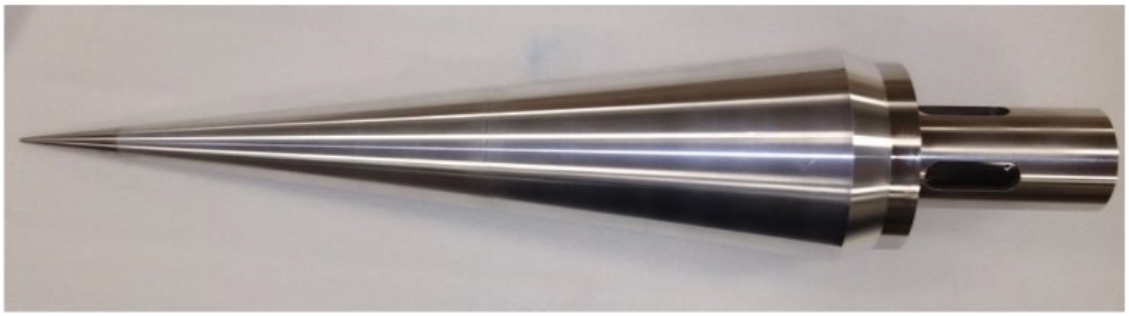

(a)

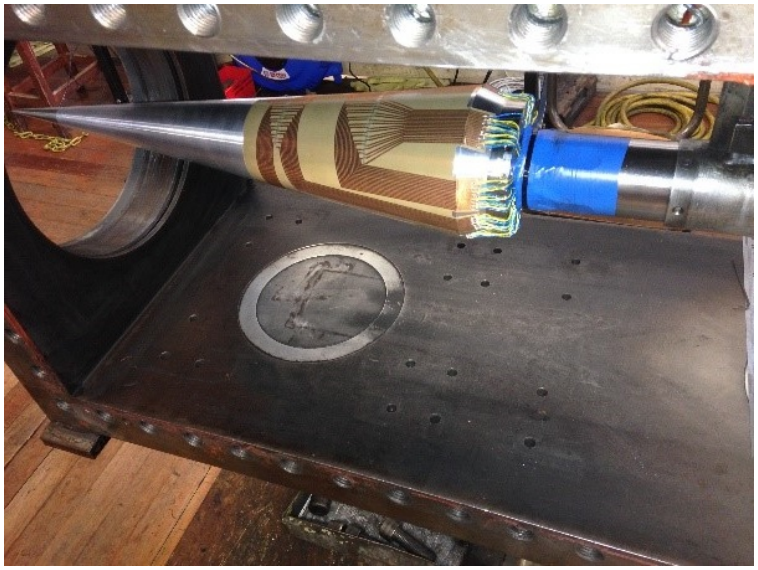

(b)

Fig. 6 Photographs of the 591-mm long 7° semi-angle blunted cone. (a) Prior to installation of the gauges. (b) After attachment of gauges and installation in the tunnel. Note that the nozzle is retracted and the sidewalls removed in the photograph.

The length and position of the model were chosen so that the cone remained within the test core of the nozzle after the nozzle had recoiled during the shots.

IV. Results

An example of the type of temperature signals that were obtained from the TFHTGs is shown in Fig. 7a. This is from a gauge in row 1 when the flow conditions were such that the boundary layer in that region was transitional. The temperature can be seen to rise about 30 K in 6 ms. Noting that the data acquisition was triggered from a nozzle-supply pressure sensor, it can be seen that there is a delay of about 250 μs from that trigger until the flow arrives at the gauge location and the temperature starts to rise. This is associated with the time it takes for starting flow to pass along the nozzle and to the location of the gauge on the model.

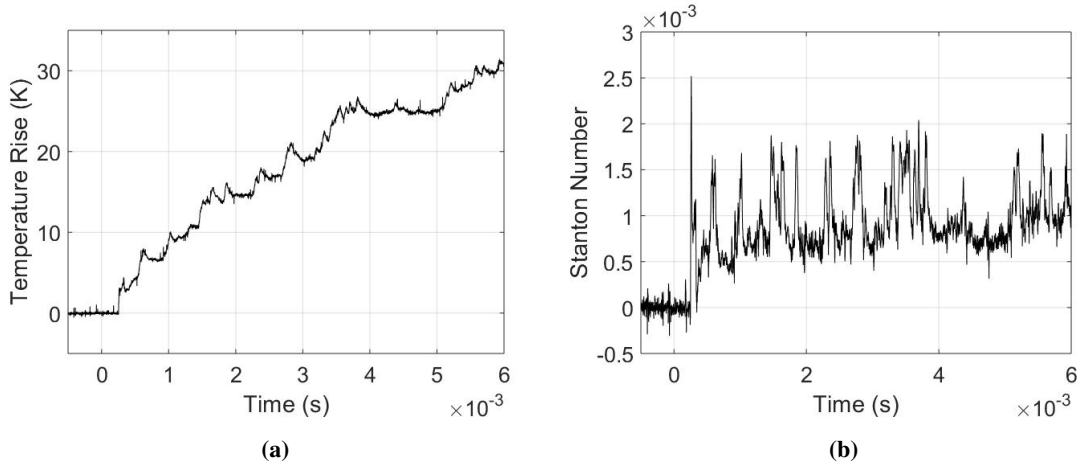

Fig. 7 Example traces from TFHTGs in a transitional region (Gauge G110, Shot 12172). (a) Temperature. (b) Heat Flux.

An indication of the signal-to-noise ratio can be seen in the temperature signal prior to flow arrival. The process of inferring the instantaneous heat-transfer rate from the temperature signal comes from solving of an inverse problem which can be very sensitive to noise on the input signal. That is the case here. Prior to flow arrival, there should be no heat transfer and therefore no change in temperature but the noise on the temperature signal is inferred to be caused by rapid increases and decreases in heat flux.

The location of transition on the cone was varied by changing the flow conditions. This included changes in the the nozzle-supply enthalpy and pressure. Heat-transfer data are presented in this paper in the form of Stanton Number. This enables the results from shots at different flow conditions to be more easily compared. The Stanton number used here is in the form,

$$\mathrm{St} = \frac{\dot{q}}{\rho_\infty u_\infty (h_s - h_w)}. \tag{1}$$

The heat-transfer signal inferred from the temperature signal in Fig. 7a is shown as the Stanton number as a function of time in Fig. 7b. The heat-transfer signal was filtered using a Savitzky-Golay smoothing filter[33]. A 3rd-order polynomial and a 21-point frame length was applied. This helps to preserve the changes in heat flux associated with the passage of turbulent spots but reduces the higher-frequency noise. Examining the signal prior to flow arrival shows that this was not fully successful in removing all the high-frequency noise. However, it can be seen that the filtered signal still shows rapid changes in Stanton number from a level of around 7×10^{-4} to around 1.4×10^{-3} as turbulent spots pass over the gauge and the heat flux jumps between laminar and turbulent levels. The same Savitzky-Golay smoothing filter was used for all of the Stanton number data presented in this paper.

The uncertainty in the measurements of heat-transfer rate due to uncertainties in thermal properties of the kapton/glue layer, the temperature coefficient of resistance of the films, and deterioration of the gauges is estimated to be 7%. The uncertainty in the Stanton number, which includes uncertainty in the heat transfer rate as well as the uncertainty in $\rho_\infty u_\infty (h_s - h_w)$ is estimated to be 13%.

The average Stanton numbers during the 2-ms test window for 11 shots are shown in Fig. 8a. The horizontal axis is the Reynolds number, based on the inviscid flow conditions calculated at the cone surface behind the shock from a 7° semi-angle cone using the method of Taylor and Maccoll [34] assuming frozen chemistry and a perfect gas, in the form,

$$\mathrm{Re}_{w_l} = \frac{\rho_w u_w l}{\mu_w}. \tag{2}$$

There are two results for each shot - one from the row of gauges at 400 mm from the apex and one from the row of gauges at 500 mm from the apex. Each point in the plot is the average Stanton number during the 2-ms test time from all gauges in a row at either 400 or 500 mm. The boundary layer was laminar at the lowest Reynolds numbers tested. The increase in Stanton number at a Reynolds number of around 2 million is associated with the start of transition. The peak in Stanton number occurs at Reynolds numbers near the end of transition and then the Stanton number slowly decreases at higher Reynolds numbers.

The intermittency of turbulence for the same 11 shots is shown in Fig. 8b. Again, each point in the plot is the average value during the test window from all gauges in a row at either 400 mm or 500 mm from the apex. A simple intermittency meter was used. The flow was deemed to be instantaneously turbulent if the heat transfer level was more than 30% of the difference between the laminar and turbulent level above the laminar level for the gauge location. It was considered to be laminar if the level was below that threshold. The laminar level was calculated using the reference-enthalpy method of Simeonides [35] and the turbulent level was calculated using van Driest II [36]. Also shown is Narasimha's universal intermittency distribution in the form

$$\gamma = 1 - e^{-0.412(\frac{\mathrm{Re}_{w_l} - \mathrm{Re}_{w_{l_t}}}{\lambda^*})^2}, \tag{3}$$

where $\mathrm{Re}_{w_{l_t}}$ is the Reynolds number at the start of transition and λ^* is the difference in Reynolds numbers between when the intermittency is 25% and 75%. i.e.

$$\lambda^* = \mathrm{Re}_{w_{l_{\gamma=0.75}}} - \mathrm{Re}_{w_{l_{\gamma=0.25}}}. \tag{4}$$

Here $\mathrm{Re}_{w_{l_t}}$ was taken to be 1.8×10^6 and λ^* to be 0.8×10^6. The results show that the intermittency rises above zero at around an Re_{w_l} of 2×10^6 and reaches unity at around an Re_{w_l} of 4×10^6. This aligns well with the mean Stanton number as a function of Re_{w_l} in Fig. 8a. There is some inevitable scatter in the data that is attributed to the limited duration (2 ms) over which the data are averaged and to unit Reynolds number effects.

Since the formation of turbulent spots is a stochastic process, there may be cases where more or fewer spots form in the region of measurement during the period of steady test flow. The point at $\mathrm{Re}_{w_l} = 4.4 \times 10^6$ is from the row of gauges at 400 mm for shot 12173 ($\mathrm{Re}_\infty = 8.7 \times 10^6$ m^{-1}). At this location there were fewer spots during the test time than there were for the points at Reynolds numbers just below and above those for this point. Therefore, the mean Stanton number and intermittency are lower than the levels for the points on either side. It is expected that the scatter due to this could be reduced with repeat shots to provide more data for each point in the plots.

There are two possible effects of unit Reynolds number on the results presented in Fig. 8. Previous transition experiments in T4 found that the transition Reynolds number increases with increasing unit Reynolds number [37]. Since the freestream Reynolds number was varied and the bluntness was kept constant in the present experiments, the Reynolds number based on the bluntness radius also varied during the tests. Changing the bluntness Reynolds number has been shown to influence the transition Reynolds number also [28]. Note in Fig. 8 that the Stanton number and intermittency are a little higher for the transitional flows at the 500 mm row than at the 400 mm row. This is consistent with later transition Reynolds numbers at higher unit Reynolds numbers. An example of this can be seen from two of the results at $\mathrm{Re}_{w_l} = 3 \times 10^6$. One result is from the 500 mm row at a unit Reynolds number of 6.2×10^6 m^{-1} (Shot 12176) and the other is from the 400-mm row at a unit Reynolds number of 7.5×10^6 m^{-1} (Shot 12175). The local Reynolds numbers at the two rows are similar but intermittency for the former is 0.67 and for the latter it is 0.48. (Contour plots of the Stanton number during the test window for these two shots are shown in Figs. 11 and 12 and discussed later.) These unit Reynolds number effects also account for some of the scatter in the results in Fig. 8.

It can be seen that a reasonable fit of the intermittency can be achieved using Eq. 3, which is based on the concentrated breakdown hypothesis.

The entropy-layer swallowing length was estimated for each condition using the method outlined in [38]. The swallowing lengths for the shots for which results are presented in this paper ranged from 150 mm, for the lowest Reynolds number condition, to 290 mm for the highest. Therefore, it is considered suitable to use Taylor-Maccoll theory to estimate the boundary-layer edge conditions between 400 and 500 mm from the virtual apex of the cone. It is known

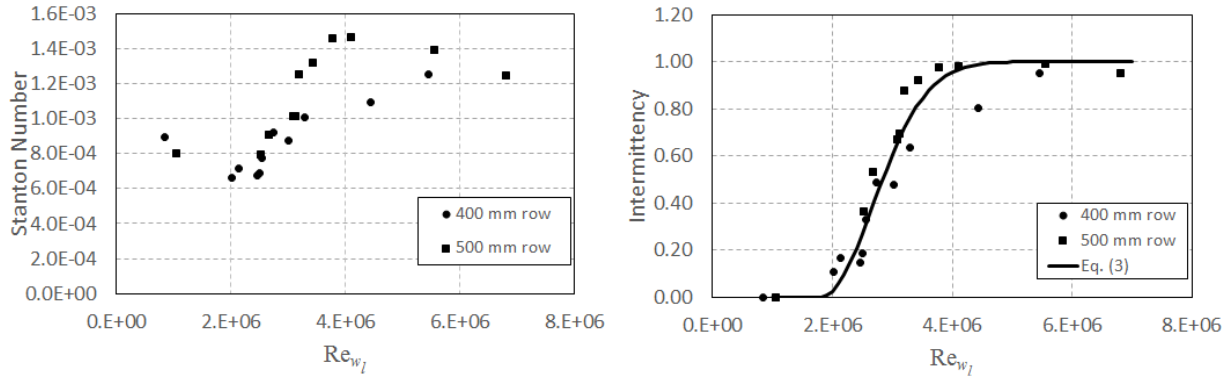

Fig. 8 Variation of parameters with Re_{w_l}. (a) Stanton Number. (b) Intermittency. Solid line is from Eq. 3 with $\mathrm{Re}_{w_{l_t}} = 1.8 \times 10^6$ and $\lambda' = 0.8 \times 10^6$.

that bluntness can affect the transition mechanism, especially when transition commences ahead of the entropy-layer swallowing length (e.g. [39]). The start of transition was not explicitly measured in the current experiments, but results in Fig. 8 indicate that the transition start location is likely to be just upstream of the swallowing length at the higher Reynolds number conditions. Therefore, there may be some effects of the nose bluntness on transition at the higher Reynolds number conditions.

At the lowest Reynolds numbers tested, the flow remained laminar at the locations of both rows of gauges. The results for $\mathrm{Re}_\infty = 2.1 \times 10^6$ m^{-1} (shot 12171) are presented in Fig. 9. The positions of the gauges are presented in terms of the angle of a ray from the apex of the cone to the centre of the gauges. Angle zero is down the centre of the array of gauges. The upper plot shows contours of Stanton number for the row at 400 mm from the apex and the lower plot is for the row at 500 mm from the apex. The circumferential distance that the gauges span at the 500-mm row is greater than at the 400-mm row but both rows span about the same range of ray angles (just under 120°).

The low Reynolds numbers were achieved by running the tunnel at relatively low nozzle-supply enthalpies and pressures. For example, the nozzle-supply enthalpy was 2.2 MJ/kg and the pressure was 4.6 MPa for shot 12171, shown in Fig. 9. The temperature rises of the gauges were relatively low (around 4 to 5 K for shot 12171) and, therefore, the signal-to-noise ratio was poorer. So the results in Fig. 9 are relatively noisy. The mean Stanton numbers are approximately 9×10^{-4} and 8×10^{-4} at the 400-mm and 500-mm rows, respectively. It can be seen that there are no large excursions to higher Stanton numbers that would be indicative of turbulent spots. The vertical straight lines that can be seen on all gauges at both rows are evidence of noise from electromagnetic interference affecting all gauges simultaneously.

Several of the 66 gauges failed during the test campaign. Also, the resistances of some of the gauges jumped during a test by an amount that was too large and rapid to be caused by heat-transfer changes. When the jumps were relatively small, it was possible to correct for them using the method outlined in [40]. In cases where a gauge had failed or the

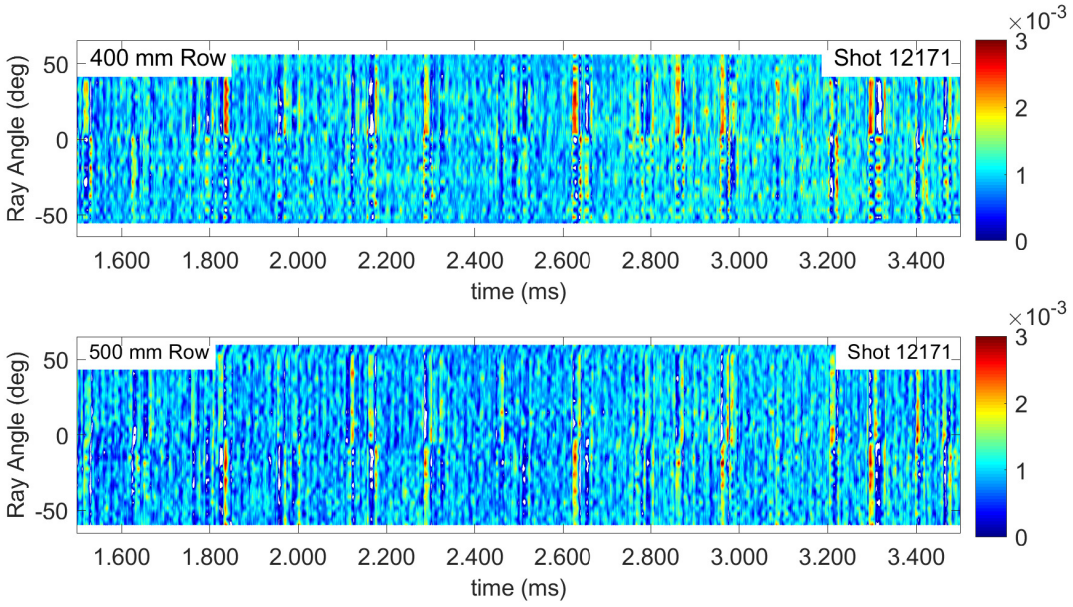

Fig. 9 Contours of instantaneous Stanton number for $Re_\infty = 2.1 \times 10^6$ m^{-1} (Shot 12171, h_s = 2.2 MJ/kg). $Re_{w_l} = 8.4 \times 10^5$ for the 400 mm row and $Re_{w_l} = 1.1 \times 10^6$ for the 500 mm row.

jumps were too large for corrections to be applied, the signals from the two gauges on either side of the failed gauge were averaged at each point in time to produce the contours of Stanton number.

The condition at the lowest Reynolds number at which turbulent spots first started forming ahead of the 400-mm row of gauges was shot 12181, when Re_∞ was 5.1×10^6 m^{-1} . The contours of Stanton number during the test time for that condition are shown in Fig. 10. The spots that have already formed at the 400-mm row of gauges are also detected at the 500-mm row. They reach that row at a later time and the spots are larger in size. The tracking of the turbulent spots from the 400-mm row to the 500-mm row for these experiments is discussed in Raghunath et al. [41]. The contours of Stanton number in Fig. 10 clearly show that there are some new spots that have formed between the two rows of gauges. This is an indication that spots are not all formed at the same streamwise location. Note that the spots are also of different sizes. This is attributed to the formation of spots at different distances into the transitional region with the smaller spots being ones that formed further along the model and have not had the chance to grow much.

Results at progressively higher unit Reynolds numbers are shown in Figs. 11 to 14. At a unit Reynolds number of 6.2×10^6 m^{-1} (Fig. 11), multiple spots have already formed at the 400-mm row. Some are larger than others. There is a period between 2.5 and 3.2 ms when there are no clear spots at the 400-mm row but many are present during the corresponding time period at the 500-mm row. So, again, there is evidence that spots form at different locations within the transitional region in the present hypersonic flows. There are similar regions where new spots have formed between the two rows of gauges in the result at $Re_\infty = 7.5 \times 10^6$ m^{-1} in Fig. 12.

When the unit Reynolds number is 8.2×10^6 m^{-1} (Fig. 13), the boundary layer at the 500-mm row is almost fully

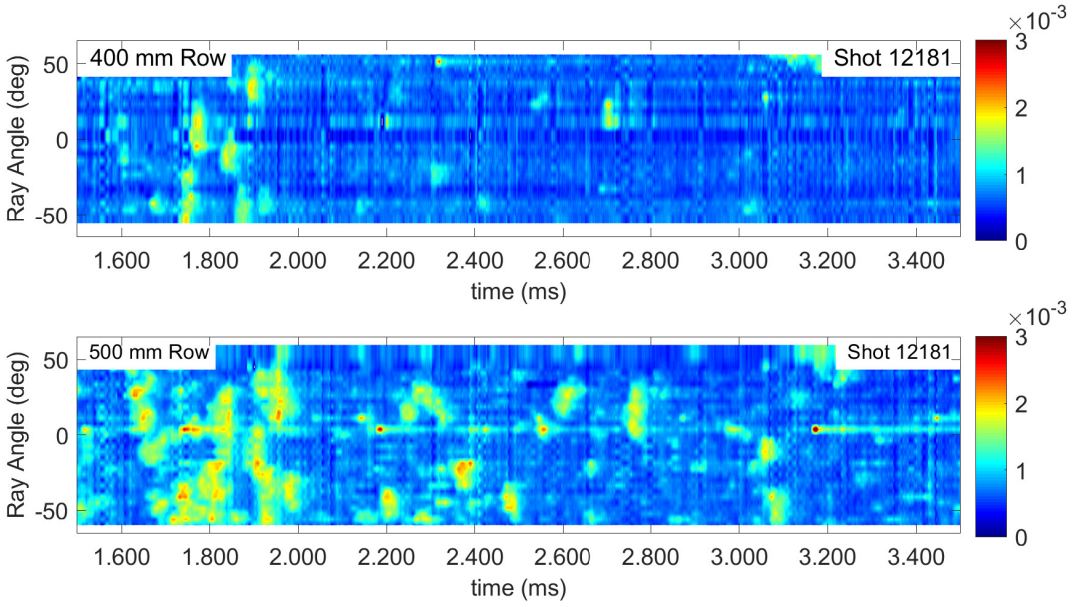

Fig. 10 Contours of instantaneous Stanton number for $Re_\infty = 5.1 \times 10^6$ m^{-1} (Shot 12181, h_s = 2.8 MJ/kg). $Re_{w_l} = 2.0 \times 10^6$ for the 400 mm row and $Re_{w_l} = 2.5 \times 10^6$ for the 500 mm row.

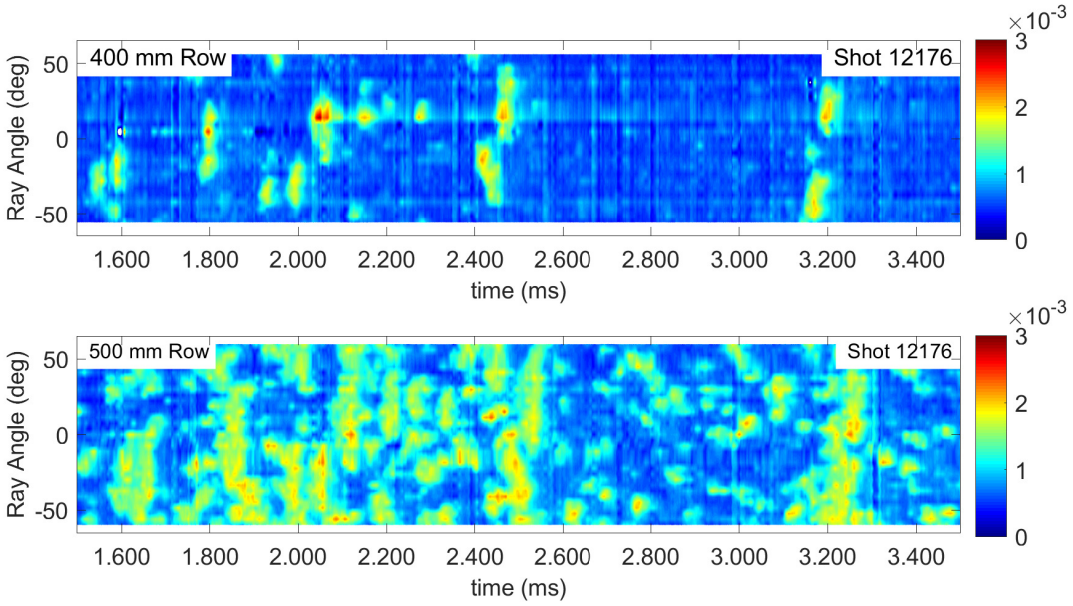

Fig. 11 Contours of instantaneous Stanton number for $Re_\infty = 6.2 \times 10^6$ m^{-1} (Shot 12176, h_s = 2.9 MJ/kg). $Re_{w_l} = 2.4 \times 10^6$ for the 400 mm row and $Re_{w_l} = 3.1 \times 10^6$ for the 500 mm row.

turbulent with only around 15 patches during the test window where the Stanton number drops to the laminar level. The fluctuations in Stanton number at the 500-mm row when the flow is not laminar are smaller at $Re_\infty = 11.1 \times 10^6$ m^{-1} (Fig. 13) than at 8.2×10^6 m^{-1} .

Animations of the contours of Stanton number at the two rows of gauges showing a 0.5-ms window for the 2-ms

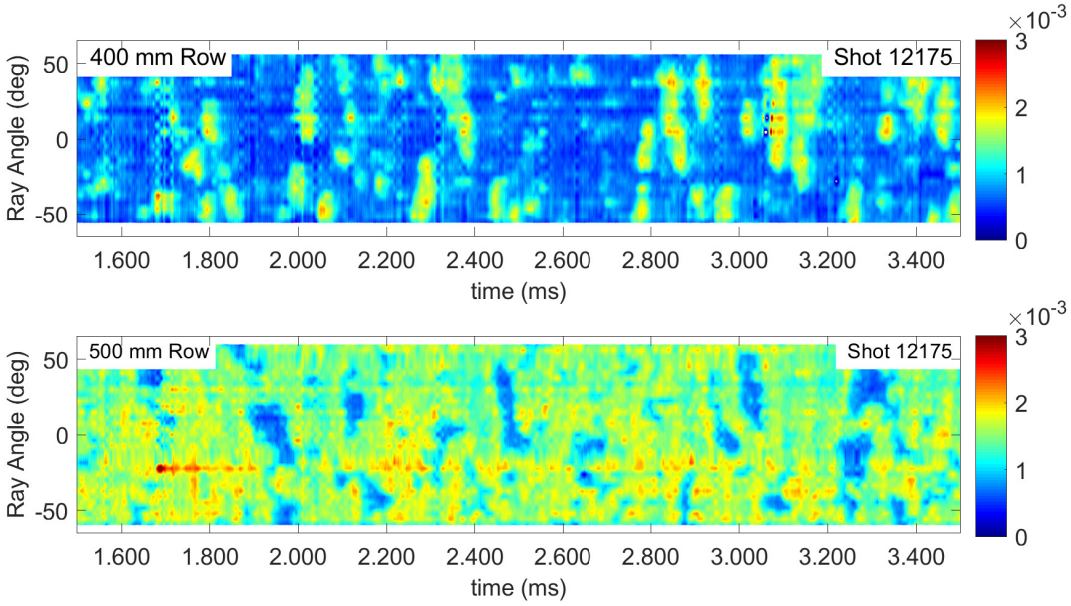

Fig. 12 Contours of instantaneous Stanton number for $\mathrm{Re}_\infty = 7.5 \times 10^6$ m^{-1} (Shot 12175, h_s = 2.5 MJ/kg). $\mathrm{Re}_{w_l} = 3.0 \times 10^6$ for the 400 mm row and $\mathrm{Re}_{w_l} = 3.8 \times 10^6$ for the 500 mm row.

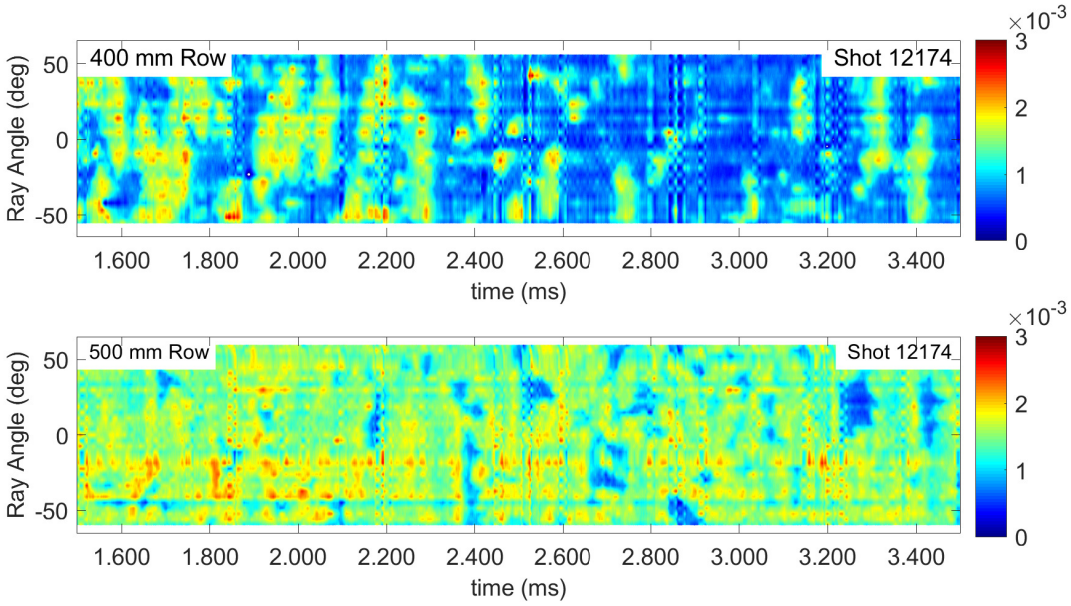

Fig. 13 Contours of instantaneous Stanton number for $\mathrm{Re}_\infty = 8.2 \times 10^6$ m^{-1} (Shot 12174, h_s = 2.2 MJ/kg). $\mathrm{Re}_{w_l} = 3.3 \times 10^6$ for the 400 mm row and $\mathrm{Re}_{w_l} = 4.1 \times 10^6$ for the 500 mm row.

duration of the test flow help visualise the formation and propagation of turbulent spots from the upstream to the downstream row. Animations for the shots shown in Figs. 9 to 14 are included in the supplementary materials for this paper. Note that these animated contour plots at each row do not show directly how spots propagate in space but comparing the results at the 400 mm row with those at the 500 mm row shows how the spots arrive later downstream

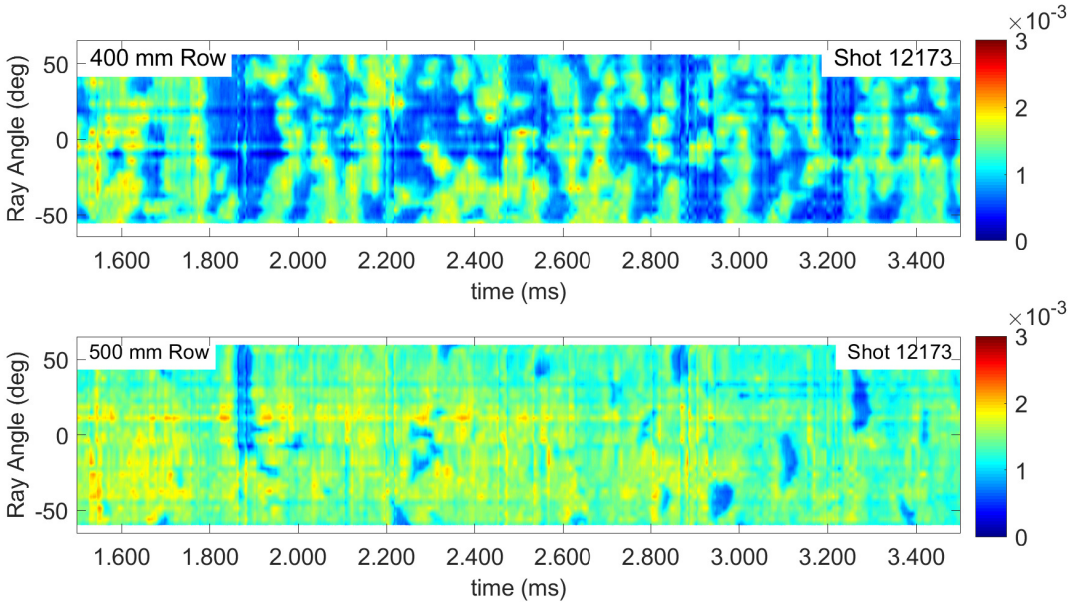

Fig. 14 Contours of instantaneous Stanton number for $\mathrm{Re}_\infty = 11.1 \times 10^6$ m^{-1} (Shot 12173, h_s = 2.4 MJ/kg). $\mathrm{Re}_{w_l} = 4.4 \times 10^6$ for the 400 mm row and $\mathrm{Re}_{w_l} = 5.5 \times 10^6$ for the 500 mm row.

and how they have grown.

V. Conclusions

The present design of closely-spaced platinum thin-film heat-transfer gauges on a kapton substrate has been found to be suitable for detecting whether or not all turbulent spots initiate within a band of small streamwise extent in the transitional flow over a blunted cone in a reflected shock tunnel. The results demonstrate that the breakdown is not strictly concentrated; turbulent spots were detected on the first row of gauges and new spots formed before the second row of gauges. The resistances of the gauges increased during the test campaign and this is attributed to erosion of the gauges due to the surface being inclined at a positive angle of attack to the oncoming flow. Coaxial thermocouple gauges would have better survivability on such surfaces but would have poorer sensitivity and it would not be possible to get the same complete rows of coverage that were achieved with the present instrumentation. A longer duration test flow or repeat tests at the same condition would help in achieving better statistics for parameters such as the intermittency of turbulence.

Funding Sources

This work was sponsored by The University of Queensland–National University of Singapore Research Collaboration.

Acknowledgments

The authors wish to thank Keith Hitchcock for maintaining T4 and Ryan Whitside, Jens Kunze, Augusto Fontan Moura and Eric Chan for assistance with running the tunnel. Thanks to Trevor Godfrey for his expertise in the manufacture of the gauges, Alex Bucknell for assistance with the design of the gauges and David Estruch-Samper for useful discussions on the design of the model.

References

[1] Fisher, M. C., "Turbulent bursts and rings on a cone in helium at Me= 7.6," *AIAA Journal*, Vol. 10, No. 10, 1972, pp. 1387, 1389. https://doi.org/10.2514/3.6637.

[2] Mee, D. J., and Goyne, C. P., "Turbulent spots in boundary layers in a free-piston shock-tunnel flow," *Shock Waves*, Vol. 6, No. 6, 1996, pp. 337–343. https://doi.org/10.1007/BF02511324.

[3] Fiala, A., Hillier, R., Mallinson, S. G., and Wijesinghe, H. S., "Heat transfer measurement of turbulent spots in a hypersonic blunt-body boundary layer," *Journal of Fluid Mechanics*, Vol. 555, 2006, pp. 81–111. https://doi.org/10.1017/S0022112006009396.

[4] Mee, D. J., and Tanguy, G., "Turbulent spot initiation rates in boundary layers in a shock tunnel," *29th International Symposium on Shock Waves 1: Volume 1*, Springer, 2015, pp. 623–628. https://doi.org/10.1007/978-3-319-16835-7_99.

[5] Jewell, J. S., Leyva, I. A., and Shepherd, J. E., "Turbulent spots in hypervelocity flow," *Experiments in Fluids*, Vol. 58, No. 4, 2017, pp. 1–14. https://doi.org/10.1007/s00348-017-2317-y.

[6] Raghunath, S., Mee, D. J., and Narasimha, R., "Estimating turbulent spot initiation rates from transition lengths in hypersonic boundary layers," *AIAA Journal*, Vol. 55, No. 11, 2017, pp. 3640–3647. https://doi.org/10.2514/1.J055502.

[7] Emmons, H. W., "The Laminar-Turbulent Transition in a Boundary Layer-Part I," *Journal of the Aeronautical Sciences*, Vol. 18, No. 7, 1951, pp. 490–498. https://doi.org/10.2514/8.2010.

[8] Johnson, M. W., and Dris, A., "The Origin of Turbulent Spots ," *Journal of Turbomachinery*, Vol. 122, No. 1, 1999, pp. 88–92. https://doi.org/10.1115/1.555431.

[9] Narasimha, R., "The laminar-turbulent transition zone in the boundary layer," *Progress in Aerospace Sciences*, Vol. 22, No. 1, 1985, pp. 29–80. https://doi.org/10.1016/0376-0421(85)90004-1.

[10] Zhang, W., Liu, P., Guo, H., Wan, M., Wang, J., and Chen, S., "Identifying the pattern of breakdown in a laminar-turbulent transition via binary sequence statistics and cellular-automaton simulations," *Phys. Rev. E*, Vol. 100, 2019, p. 023110. https://doi.org/10.1103/PhysRevE.100.023110.

[11] Gostelow, J. P., Walker, G. J., Solomon, W. J., Hong, G., and Melwani, N., "Investigation of the Calmed Region Behind a Turbulent Spot," *Journal of Turbomachinery*, Vol. 119, No. 4, 1997, pp. 802–809. https://doi.org/10.1115/1.2841191.

[12] Schultz, D. L., and Jones, T. V., "Heat-transfer measurements in short-duration hypersonic facilities," Tech. rep., ADVISORY GROUP FOR AEROSPACE RESEARCH AND DEVELOPMENT, AGARDograph 165, 1973.

[13] Alam, T., and Kumar, R., "A review on thin film fast response heat transfer gauges," *Review of Scientific Instruments*, Vol. 92, No. 3, 2021, p. 031501. https://doi.org/10.1063/5.0015932.

[14] Clark, J. P., Jones, T. V., and LaGraff, J. E., "On the propagation of naturally-occurring turbulent spots," *Journal of Engineering Mathematics*, Vol. 28, No. 1, 1994, pp. 1–19. https://doi.org/10.1007/BF02383602.

[15] Anthony, R. J., Jones, T. V., and LaGraff, J. E., "Visualization of transitional boundary Layer heat flux using high density thin film arrays," *39th Aerospace Sciences Meeting and Exhibit*, AIAA-2001-553, 2001. https://doi.org/10.2514/6.2001-553.

[16] Mee, D. J., "Boundary-layer transition measurements in hypervelocity flows in a shock tunnel," *AIAA journal*, Vol. 40, No. 8, 2002, pp. 1542–1548. https://doi.org/10.2514/2.1851.

[17] Ozawa, H., Laurence, S. J., Schramm, J. M., Wagner, A., and Hannemann, K., "Fast-response temperature-sensitive-paint measurements on a hypersonic transition cone," *Experiments in Fluids*, Vol. 56, No. 1, 2015, pp. 1–13. https://doi.org/10.1007/s00348-014-1853-y.

[18] Chynoweth, B. C., Schneider, S. P., Hader, C., Fasel, H., Batista, A., Kuehl, J., Juliano, T. J., and Wheaton, B. M., "History and progress of boundary-layer transition on a Mach-6 flared cone," *Journal of Spacecraft and Rockets*, Vol. 56, No. 2, 2019, pp. 333–346. https://doi.org/10.2514/1.A34285.

[19] Pandey, A., Casper, K. M., Flood, J. T., Bhakta, R., Spillers, R., and Beresh, S. J., "Tracking Turbulent Spots on a Hypersonic Cone at Angle of Attack using Temperature-Sensitive Paint," *AIAA Aviation 2021 Forum*, AIAA-2021-2889, 2021. https://doi.org/10.2514/6.2021-2889.

[20] Anthony, R. J., Oldfield, M. L. G., Jones, T. V., and LaGraff, J. E., "Development of high-density arrays of thin film heat transfer gauges," *Proceedings of the 5th ASME/JSME Thermal Engineering Joint Conference*, AJTE99-6159, 1999.

[21] Collins, M., Chana, K., and Povey, T., "New technique for the fabrication of miniature thin film heat flux gauges," *Measurement science and technology*, Vol. 26, No. 2, 2015, p. 025303. https://doi.org/10.1088/0957-0233/26/2/025303.

[22] Piccini, E., Guo, S. M., and Jones, T. V., "The development of a new direct-heat-flux gauge for heat-transfer facilities," *Measurement Science and Technology*, Vol. 11, No. 4, 2000, p. 342. https://doi.org/10.1088/0957-0233/11/4/302.

[23] Oldfield, M. L. G., "Impulse Response Processing of Transient Heat Transfer Gauge Signals," *Journal of Turbomachinery*, Vol. 130, No. 2, 2008. https://doi.org/10.1115/1.2752188, 021023.

[24] Hannemann, K., Itoh, K., Mee, D. J., and Hornung, H. G., "Free Piston Shock Tunnels HEG, HIEST, T4 and T5," *Experimental Methods of Shock Wave Research*, edited by O. Igra and F. Seiler, Springer International Publishing, Cham, 2016, pp. 181–264. https://doi.org/10.1007/978-3-319-23745-9_7.

[25] Chan, W. Y. K., Smart, M. K., and Jacobs, P. A., "Flowpath Design of an Axisymmetric Mach 7.0 Nozzle for T4," Research Report 2013/01, School of Mechanical and Mining Engineering, The University of Queensland, Brisbane, Australia, 2014.

[26] Chan, W. Y. K., Smart, M. K., and Jacobs, P. A., "Experimental validation of the T4 Mach 7.0 nozzle," Research Report 2014/14, School of Mechanical and Mining Engineering, The University of Queensland, Brisbane, Australia, 2014.

[27] Jacobs, P. A., Gollan, R. J., Potter, D. F., Zander, F., Gildfind, D. E., Blyton, P., Chan, W. Y. K., and Doherty, L., "Estimation of high-enthalpy flow conditions for simple shock and expansion processes using the ESTCj program and library," *Mechanical Engineering Report 2011/02, School of Mechanical and Mining Engineering, The University of Queensland, Brisbane, Australia*, 2014.

[28] Schneider, S. P., "Hypersonic laminar–turbulent transition on circular cones and scramjet forebodies," *Progress in Aerospace Sciences*, Vol. 40, No. 1-2, 2004, pp. 1–50. https://doi.org/10.1016/j.paerosci.2003.11.001.

[29] Ramprakash, A., "Experimental Investigation of Noise Generated in a Scramjet Engine," Ph.D. thesis, The University of Queensland, Submitted., 2023.

[30] Jewell, J. S., Parziale, N. J., Leyva, I. A., and Shepherd, J. E., "Effects of shock-tube cleanliness on hypersonic boundary layer transition at high enthalpy," *AIAA journal*, Vol. 55, No. 1, 2017, pp. 332–338. https://doi.org/10.2514/1.J054897.

[31] Fedorov, A. V., "Receptivity of a supersonic boundary layer to solid particulates," *Journal of Fluid Mechanics*, Vol. 737, 2013, p. 105–131. https://doi.org/10.1017/jfm.2013.564.

[32] Stanfield, S. A., Kimmel, R. L., Adamczak, D., and Juliano, T. J., "Boundary-layer transition experiment during reentry of HIFiRE-1," *Journal of Spacecraft and Rockets*, Vol. 52, No. 3, 2015, pp. 637–649. https://doi.org/10.2514/1.A33197.

[33] Press, W. H., and Teukolsky, S. A., "Savitzky-Golay smoothing filters," *Computers in Physics*, Vol. 4, No. 6, 1990, pp. 669–672. https://doi.org/10.1063/1.4822961.

[34] Taylor, G. I., and Maccoll, J. W., "The air pressure on a cone moving at high speeds.—II," *Proceedings of the Royal Society of London. Series A*, Vol. 139, No. 838, 1933, pp. 298–311. https://doi.org/10.1098/rspa.1933.0018.

[35] Simeonides, G., "Generalized reference enthalpy formulations and simulation of viscous effects in hypersonic flow," *Shock Waves*, Vol. 8, No. 3, 1998, pp. 161–172. https://doi.org/10.1007/s001930050109.

[36] van Driest, E. R., "The problem of aerodynamic heating," *Aeronautical Engineering Review*, Vol. 15, No. 10, 1956, pp. 26–41.

[37] He, Y., and Morgan, R. G., "Transition of compressible high enthalpy boundary layer flow over a flat plate," *The Aeronautical Journal*, Vol. 98, No. 972, 1994, pp. 25–34. https://doi.org/10.1017/S0001924000050181.

[38] Stetson, K., "Nosetip bluntness effects on cone frustum boundary layer transition in hypersonic flow," *16th Fluid and Plasmadynamics Conference*, AIAA-83-1763, 1983. https://doi.org/10.2514/6.1983-1763.

[39] Marineau, E. C., Moraru, G. C., Lewis, D. R., Norris, J. D., Lafferty, J. F., Wagnild, R. M., and Smith, J. A., "Mach 10 boundary layer transition experiments on sharp and blunted cones," *19th AIAA International Space Planes and Hypersonic Systems and Technologies Conference*, AIAA-2014-3108, 2014. https://doi.org/doi.org/10.2514/6.2014-3108.

[40] Convery-Brien, I., "Characteristics of Turbulent Spots and the Transition Zone Under the Influence of an Adverse Pressure Gradient Within a Free Piston Shock Tunnel," Master's thesis, The University of Queensland, 2020. https://doi.org/10.14264/5778aac.

[41] Raghunath, S., Khoo, B. C., and Mee, D. J., "Characteristics of turbulent spots in a hypersonic transitional boundary layer inferred from dense arrays of thin-film heat transfer gauges," *Proceedings of the 32nd International Symposium on Shock Waves (ISSW32 2019)*, Springer, Singapore, 2019, pp. 2255–2263. https://doi.org/10.3850/978-981-11-2730-4_0359.